Proceedings of ISFA2016
2016 International Symposium on Flexible Automation
Cleveland, Ohio, U.S.A., 1 - 3 August, 2016

MODELING AND OBSERVER-BASED COMPENSATION OF SLIP IN A FRICTION DRIVE FOR SERVO POSITIONING

Molong Duan
Department of Mechanical Engineering
University of Michigan, Ann Arbor
G.G. Brown Laboratory, 2350 Hayward
Ann Arbor, MI, 48109
molong@umich.edu

Chinedum E. Okwudire
Department of Mechanical Engineering
University of Michigan, Ann Arbor
G.G. Brown Laboratory, 2350 Hayward
Ann Arbor, MI, 48109
okwudire@umich.edu

ABSTRACT

This paper studies slip in friction drives in the context of a precision servo positioner equipped with a twist-roller friction drive. The servo positioner is modeled using a two-mass model that includes the experimentally-identified nonlinear slip dynamics of the friction drive. The model is then used to design an observer-based compensation scheme aimed at reducing the slip-induced performance degradation of the servo positioner's linear time invariant controller. The compensation scheme is validated in simulations and experiments using state feedback controllers. Tracking performance with the proposed slip compensation scheme, compared with the original controller and an intuitive high pass filter approach, is shown to improve considerably.

NOMENCLATURE

Symbol	Description
$\mathbf{A}$, $\mathbf{B}_u$, $\mathbf{B}_d$, $\mathbf{B}_n$, $\mathbf{C}_y$	system's linear dynamics matrices
F_L, F_t, F_f	load, transmitted and friction forces
$\mathbf{G}$	linear two-mass system transfer function
$\mathbf{K}$, $\mathbf{L}$	feedback, observer gain matrices
$\mathbf{Q}$, R	weights in LQR control
$\mathbf{Y}$	reference compensation block
X_{lim},V_{lim},A_{lim},J_{lim},S_{lim}	reference trajectory parameters
b_1, b_2, c, k	two-mass model damping and stiffness
d, u	disturbance, control input
$\mathbf{f}$	general model nonlinearity
f_s	slip rate function
l, l_0	lead, critical lead parameter
m_1, m_2	driving, driven component masses
p, p_0, p_1, p_2	slip coefficients
r	revolution of shaft
s_r	slip per revolution
v	velocity used in identification
x_1, x_2	displacements of driving, driven masses
x_r	reference trajectory of driven mass
x_s, $\mathbf{y}_s$	slip displacement, compensation term
$\mathbf{y}$, $\mathbf{z}$	system outputs, states
$\mathbf{y}_r$	compensated reference trajectory
γ	Lipschitz constant
Ω	set of admissible states

1. INTRODUCTION

A friction drive is a type of transmission system that depends on friction between contacting surfaces to transmit motion. Friction drives are used in various applications including automotive [1], robotics [2], manufacturing machines [3–5] and astronomical instrumentations [6]. When used in servo positioning systems, friction drives can be categorized into two major types: repetitive and continuous friction drives. Repetitive friction drives are usually actuated by short range, high frequency actuators. By repetitively changing their contact condition, incremental micro stepping is accumulated into macro motion [7–9]. On the contrary, continuous friction drives maintain constant contact such that motion is transmitted continuously [3,10,11].

Slip is a common occurrence in friction drives [3,5,12]. It is exploited in the design of repetitive friction drives where, by manipulating stick-slip dynamics, accumulation of short range but high frequency motion is achieved [7,9]. However, slip is often undesirable in continuous friction drives because it can adversely influence positioning performance [12].

One way of minimizing slip is to design continuous friction drives with an optimal level of normal force between contacting surfaces [13]. Feedback control can also be used to (further) mitigate slip. In many precision servo positioners that experience slip, feedback control is achieved using position outputs measured from the driven side of the servo positioner [3,11,14]. While this approach helps to ensure the precise positioning of the load, it suffers from potential loss of feedback performance due to non-collocation of the sensor and actuator [15]. More importantly, this approach neglects slip dynamics, which could cause transmission instability, for instance when the

978-1-5090-3466-6/16/$31.00 ©2016 IEEE

reference trajectory reaches the critical frequency derived in [16]. One approach for addressing performance degradation due to unmodeled nonlinearities (like slip) is to use an internal model control, as proposed in [10]. This approach is however limited to well-damped and minimum phase systems, since it needs to invert the system dynamics. Also, it uses feedback only from the driven side, and is limited to low speed applications. A control scheme using feedback from both the driving and driven sides is realized in [17] through slip estimation. The slip estimate is modeled as velocity loss, and can therefore only be used to statically compensate the velocity command. Moreover, the method is not robust to slip parameter variation.

In the context of a specific twist-roller friction drive [18], this paper proposes a method for identifying and compensating slip in continuous friction drives using a nonlinear observer. The proposed control scheme makes use of feedback from the driving and driven sides of the servo positioner, and is shown in simulations and experiments to significantly improve positioning performance, while remaining robust to variations in slip model parameters. In Section 2, the friction drive is modeled and its slip dynamics is experimentally identified. The model is used in Section 3 to design a nonlinear observer for compensating slip. In Section 4, the proposed method is validated through simulations and experiments, followed in Section 5 by conclusions and future work.

2. MODELING

2.1 Friction Based Two Mass Model

The two-mass model is widely used to model servo positioning systems that have inherent transmission mechanisms [19]. It connects the driving and driven components of the transmission with a spring and damper, as shown in Fig. 1(a). Mathematically, the two-mass model can be expressed as

$$\begin{aligned} m_1\ddot{x}_1 + b_1\dot{x}_1 + c(\dot{x}_1 - \dot{x}_2) + k(x_1 - x_2) &= u \\ m_2\ddot{x}_2 + b_2\dot{x}_2 + c(\dot{x}_2 - \dot{x}_1) + k(x_2 - x_1) &= d \end{aligned} \tag{1}$$

where m_1 and m_2 respectively represent the (equivalent) masses of the driving and driven components; x_1 and x_2 are the displacements of the two masses (x_2 is usually the target for control); k, c, b_1, b_2 are the stiffness, damping and rigid body damping coefficients of the system; u is the control and d is the disturbance input. The system in Fig. 1(a) assumes that the control and disturbance inputs are on different sides of the transmission. This assumption is valid since m_2 is usually the component interacting with the uncertain physical load and the disturbance on the actuator side is usually known and thus can be pre-compensated. Note that the transmission ratio is inherent in the two-mass formulation, meaning that some of its parameters are rescaled by the transmission ratio [18–20].

Friction drives resemble traditional geared drives with respect to their transmission ratio [20]. However, in friction drives, the relative displacement between x_1 and x_2 arises from a combination of the elastic deformation of the transmission (i.e., k) and the accumulated slip during its operation. Failure to capture the relative displacement due to slip may lead to performance degradation and even instability [16].

In order to model slip, similar to the plastic module introduced in [1,21], a massless plate is added to the traditional two-mass model as in Fig. 1(b); the plate is attached to m_1, whose relative displacement is modeled as the slip state, x_s, representing the slip in the transmission. Accordingly, Eq. (1) is re-written as

$$\begin{aligned} m_1\ddot{x}_1 + b_1\dot{x}_1 &= u - F_t \\ m_2\ddot{x}_2 + b_2\dot{x}_2 &= d + F_t \end{aligned} \tag{2}$$

with the transmitted force between m_1 and m_2 modeled as

$$F_t = k\left(x_1 - x_2 + x_s\right) + c\left(\dot{x}_1 - \dot{x}_2 + \dot{x}_s\right) \tag{3}$$

In the most general case, we assume that the slip rate is a function of all system states; i.e.,

$$\dot{x}_s = f_s\left(x_1, x_2, \dot{x}_1, \dot{x}_2, x_s, \dot{x}_s\right) \tag{4}$$

Note that in Eq. (4) there is the possibility of an algebraic loop, since f_s is unknown. As will be shown in Section 2.3, the algebraic loop can be resolved through the model of f_s. By defining a state vector $\mathbf{z}$ combining the position, velocity and slip variables, the overall system dynamics can be decomposed to a linear and nonlinear part:

$$\frac{d}{dt}\underbrace{\begin{bmatrix} x_1 \\ x_2 \\ \dot{x}_1 \\ \dot{x}_2 \\ x_s \end{bmatrix}}_{\triangleq \mathbf{z}} = \underbrace{\mathbf{A}\begin{bmatrix} x_1 \\ x_2 \\ \dot{x}_1 \\ \dot{x}_2 \\ x_s \end{bmatrix} + \overbrace{\begin{bmatrix} 0 \\ 0 \\ \frac{1}{m_1} \\ 0 \\ 0 \end{bmatrix}}^{\triangleq \mathbf{B}_u} u + \overbrace{\begin{bmatrix} 0 \\ 0 \\ 0 \\ \frac{1}{m_2} \\ 0 \end{bmatrix}}^{\triangleq \mathbf{B}_d} d}_{\text{Linear}} + \overbrace{\begin{bmatrix} 0 \\ 0 \\ \frac{-c}{m_1} \\ \frac{c}{m_2} \\ 1 \end{bmatrix}}^{\triangleq \mathbf{B}_n} \underbrace{f_s}_{\text{Nonlinear}} \tag{5}$$

$$\mathbf{y} = \underbrace{\left[\mathbf{I}_{4\times4} \mid \mathbf{0}_{4\times1}\right]}_{\triangleq \mathbf{C}_y}\mathbf{z}$$

where

$$\mathbf{A} \triangleq \begin{bmatrix} 0 & 0 & 1 & 0 & 0 \\ 0 & 0 & 0 & 1 & 0 \\ -\frac{k}{m_1} & \frac{k}{m_1} & -\frac{c+b_1}{m_1} & \frac{c}{m_1} & -\frac{k}{m_1} \\ \frac{k}{m_2} & -\frac{k}{m_2} & \frac{c}{m_2} & -\frac{c+b_2}{m_2} & \frac{k}{m_2} \\ 0 & 0 & 0 & 0 & 0 \end{bmatrix} \tag{6}$$

Output vector $\mathbf{y} = [y_1, y_2, y_3, y_4]^T$ represents the accessible states obtained through a selection matrix $\mathbf{C}_y$. Matrices $\mathbf{A}$, $\mathbf{B}_u$, $\mathbf{B}_d$, $\mathbf{B}_n$ are defined as in Eqs. (5) and (6). The slip dynamics, f_s, is the nonlinear component in the equation; it can be identified experimentally for a given servo positioner, as is demonstrated in the following sub-sections.

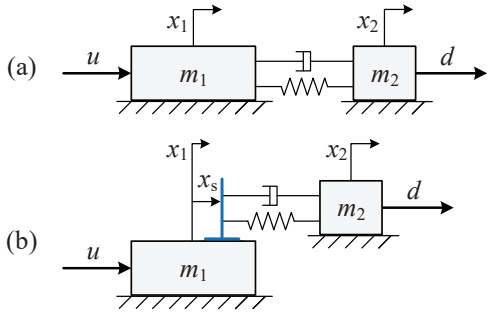

Figure 1: (a) Original Two-Mass Model and (b) Two-Mass Model with Slip

2.2 Overview of Servo Positioner

Figure 2 shows the schematic of the precision servo positioner that is used in this paper to demonstrate the modeling and compensation of slip. It is a redundantly actuated hybrid feed drive (HFD) [18,20] consisting of a linear motor, and a rotary motor which generates linear motion via a Roh'lix® nut (i.e., a twist-roller friction drive). As described in [18], the HFD is equipped with the twist-roller friction drive (TRFD) to facilitate rapid (dis)engagement of the nut from the smooth shaft, with the help of a toggle mechanism and pneumatic pistons. This allows the HFD to have two modes of operation – i.e., a rapid positioning mode where the nut is disengaged and the linear motor drives the table, and a cutting mode where the nut is engaged and the rotary motor drives the table (assisted by the linear motor). The HFD is thus able to realize extremely fast rapid positioning as well as precise and energy efficient motion under high cutting (i.e., machining) loads [18,20].

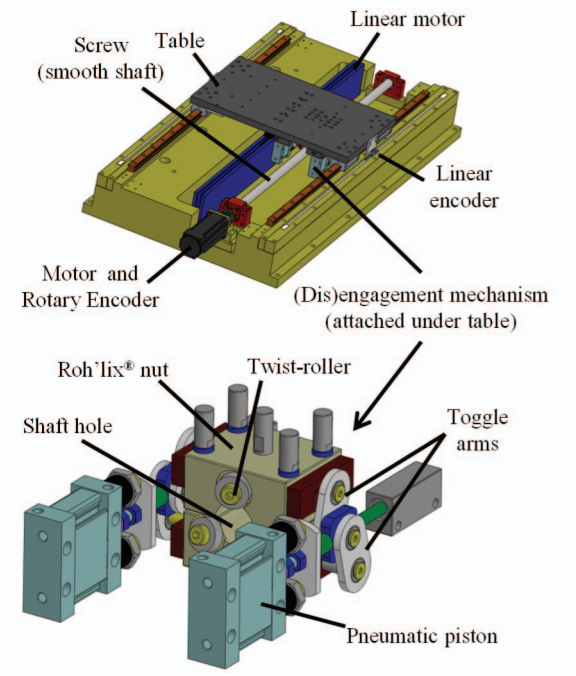

Figure 2: Servo Positioner (Hybrid Feed Drive) with Twist-Roller Friction Drive

The precision requirements for the HFD during cutting are very stringent. Therefore, the slip experienced by the TRFD during the cutting mode must be mitigated. Prior work by the authors [18,20] relied on the linear motor to compensate slip by brute force, which could lead to excessive wear of the smooth shaft and losses in efficiency. It is therefore desired in this paper to compensate slip using the rotary motor, with the help of a model of slip and a slip observer that makes use of feedback from the linear and rotary encoders of the HFD.

2.3 Model Identification of Slip for TRFD

Slip in continuous friction drives has been experimentally observed to be largely related to surface contact conditions [3,6,16] (e.g., surface speed, normal force, thrust force and lubrication). The normal force and lubrication conditions of the HFD's TRFD can be regarded as uniform. However, its transmitted (i.e., thrust) force and surface speed are variables that depend a lot on machining conditions. Therefore we can simplify the nonlinear slip dynamics in Eq. (4) to

$$\dot{x}_s = f_s\left(F_t, \dot{x}_1\right) \tag{7}$$

where $\dot{x}_1$ is the velocity of m_1 and F_t is force transmitted through the TRFD (which depends on the states of the two-mass model). Note that either $\dot{x}_1$ or $\dot{x}_2$ can be used in Eq. (7) to represent surface speed, because the velocity difference between m_1 and m_2 is small compared to their nominal value. Here we chose $\dot{x}_1$ because it is easier to control m_1 to achieve high speeds due to the collocation of feedback and control input (i.e., the rotary encoder and rotary motor). Moreover, the equivalent mass m_1 is much larger than m_2 due to the mechanical advantage of the TRFD; thus $\dot{x}_1$ is less oscillatory compared to $\dot{x}_2$ which could benefit the observer designed in Section 3.

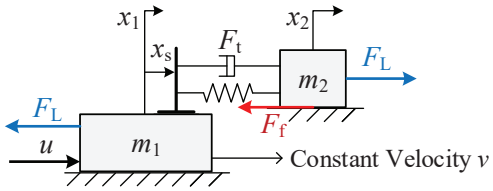

Figure 3: Constant Velocity Slip Test Setup

Figure 3 shows a schematic of the test setup for identifying slip in the TRFD. Counteracting forces F_L are applied to the system through the two actuators of the HFD, and m_1 is controlled with the rotary motor (u) to maintain a constant velocity $\dot{x}_1 = v$. Considering slip as a form of lead error [3], given long enough traversal time, the positioning difference $x_1 - x_2$ will be dominated by x_s, which would linearly increase with time. Thus, the slip dynamics, f_s, can be approximated as the rate of slip accumulation (or slip rate); i.e., $\Delta(x_1 - x_2)/\Delta t$.

Note from Fig. 3 that the transmitted force, F_t, is related to the applied load, F_L, by

$$F_t = F_L - F_f \tag{8}$$

where F_f is the friction force on m_2, which can be identified experimentally by disengaging the Roh'lix® nut from the shaft and measuring the linear motor's force for constant velocity tracking. Using this information, the transmitted force's influence on slip rate under different velocities is shown in Fig. 4, from which the following observations can be made:

i) The slip rate in constant velocity tracking is constant (every data point on Fig. 4 represents the constant slip rate measured for each velocity and transmitted force).
ii) The slip rate is almost linearly dependent on velocity and transmitted force.
iii) The linear relationship is slightly different for cases when the transmitted force and velocity are of the same or different directions.

With these observations, we can represent slip rate as a bilinear equation of the velocity and transmitted force by introducing a new variable called slip per revolution, s_r, given by

$$s_r \triangleq \frac{dx_s}{dr} = \dot{x}_s \frac{dt}{dr} = \frac{\dot{x}_s}{\dot{x}_1} l \tag{9}$$

where l represents the (nominal) lead of the TRFD and r represents the number of revolutions of the shaft, given by

$$r = x_1 / l \tag{10}$$

Accordingly, the slip dynamics can be expressed as

$$\dot{x}_s = f_s = \frac{1}{l} s_r(F_t)\dot{x}_1 \tag{11}$$

Based on the third observation from Fig. 4, the relationship between s_r and F_t can be expressed as piecewise linear; i.e.,

$$s_r(F_t) = \begin{cases} p_1 F_t & \text{when } F_t \dot{x}_1 \geq 0 \\ p_2 F_t & \text{when } F_t \dot{x}_1 < 0 \end{cases} \tag{12}$$

having two modes, namely the dragging mode ($F_t \dot{x}_1 \geq 0$) and the compressing mode ($F_t \dot{x}_1 < 0$). It is also useful, for the sake of simplicity, to consider a uniform linear model which ignores the two modes; i.e.,

$$s_r(F_t) = p_0 F_t \tag{13}$$

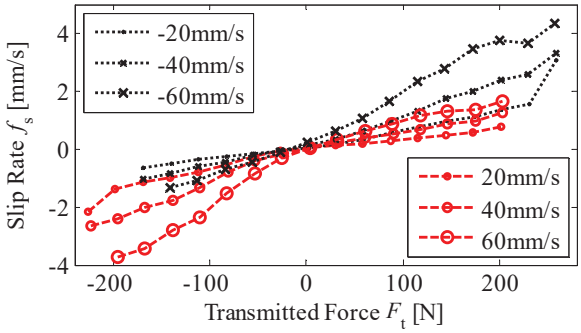

Figure 4: Results of Slip Rate Experiments

Figure 5 shows the experimentally identified slip per revolution for various velocities as functions of transmitted force. The red dots represent measured slip per revolution for positive velocities while the black crosses are for negative velocities. The green line presents the uniform linear model of Eq. (13) which fits all the data points. The blue lines represent the two modes of the piecewise linear model as in Eq. (12). The identified slip coefficients, p_0, p_1 and p_2, and their corresponding coefficients of determination (i.e. R^2) are listed in Tab. 1. While the piecewise linear model does a very good job of explaining the data, the uniform linear model is seen to not be very far off.

Table 1: Identified Slip Coefficients

	p_0	p_1	p_2
Estimation[mm·rev^{-1}·N^{-1}]	1.2×10^{-3}	7.7×10^{-4}	1.6×10^{-3}
R^2	0.89	0.95	0.98

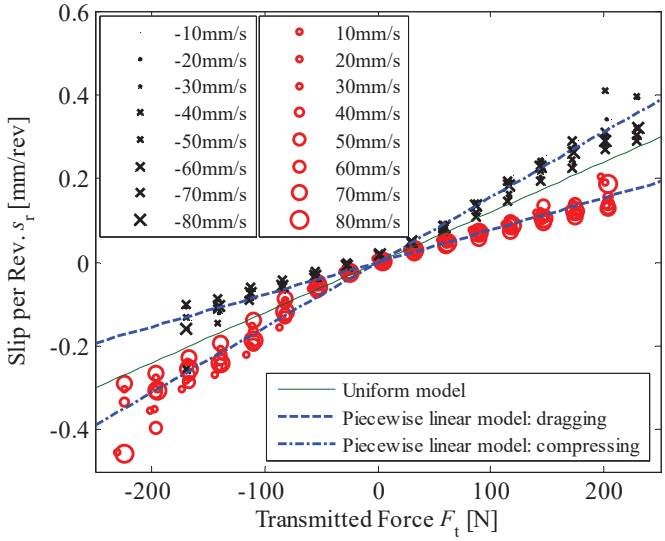

Figure 5: Relationship between Slip Rate and Transmitted Force at Different Velocities

Though the slip model is derived based on steady state velocity tracking, it is very meaningful for the HFD, since machining typically occurs at constant velocity. Moreover, the fact that the model is linear can be used to eliminate the algebraic loop that is inherent in Eq. (7) (since $\dot{x}_s$ and F_t are mutually dependent). To do this, let us use p to represent any of the slip coefficients, p_i ($i = 0,1,2$), in Eqs. (12) and (13). Combining Eqs. (3) and (11), the slip dynamics becomes

$$\begin{aligned} \dot{x}_s &= \frac{p\dot{x}_1}{l}\left[k\left(x_1 - x_2 + x_s\right) + c\left(\dot{x}_1 - \dot{x}_2 + \dot{x}_s\right)\right] \\ \Rightarrow \dot{x}_s &= \frac{p\dot{x}_1\left[k\left(x_1 - x_2 + x_s\right) + c\left(\dot{x}_1 - \dot{x}_2\right)\right]}{l - pc\dot{x}_1} = f_s \end{aligned} \tag{14}$$

which is a state dependent nonlinear function that breaks the algebraic loop in f_s. The denominator of the nonlinear function, expressed as

$$l_0 = l - pc\dot{x}_1 \tag{15}$$

is a crucial parameter since it can introduce mathematical singularity in the slip model. When $l_0 \approx 0$ (i.e., $l \approx pc\dot{x}_1$) the TRFD loses its controllability of m_2. Note that l_0/l can be viewed as an indicator of transmission efficiency, which should be

maintained as close as possible to unity; this can be practically achieved by reducing p or $\dot{x}_1$.

Apart from the newly added slip component, the rest of the HFD's two-mass model can be identified using standard frequency response experiments. The excitation amplitudes used for the frequency response measurements are large enough such that x_s is small compared to x_1 and x_2. Therefore, slip can be ignored, resulting in the equation

$$\begin{bmatrix} x_1 \\ x_2 \end{bmatrix} \approx \mathbf{G}(s) \begin{bmatrix} u \\ d \end{bmatrix} \tag{16}$$

where $\mathbf{G}$ is the transfer function of the original two mass model. Sinusoidal signals u and d are applied to the HFD and the magnitude and phase of their responses are measured [20]. Figure 6 shows the magnitude information of the measured frequency response function and the fitted linear model. The identified model parameters are summarized in Tab. 2.

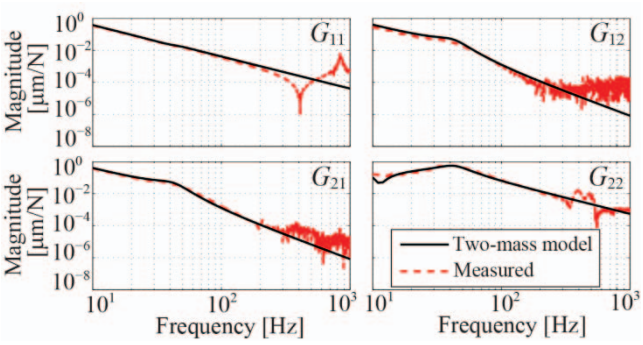

Figure 6: Two-Mass Model Identification

Table 2: Identified Parameters of Two-mass Model

m_1 [kg]	m_2 [kg]	b_1 [kg/s]	b_2 [kg/s]	c [kg/s]	k [N/μm]
639.2	44.3	3456.4	2.3	4686.8	6.8443

3. OBSERVER BASED SLIP COMPENSATION

3.1 Conditions for Observer Design

The extended Luenberger observer can be used to observe states of systems with nonlinear dynamics [22], like the slip state, x_s. However, the Lipschitz condition must be satisfied by the observer to ensure convergence of its errors which partly arise from the nonlinear terms in the system dynamics [22,23]. The Lipschitz condition holds for a nonlinear function $\mathbf{f}(\mathbf{z})$ if there exists a positive γ satisfying

$$\left\|\mathbf{f}(\mathbf{z}_a) - \mathbf{f}(\mathbf{z}_b)\right\| \le \gamma \left\|\mathbf{z}_a - \mathbf{z}_b\right\| \tag{17}$$

where $\mathbf{z}_a$ and $\mathbf{z}_b$ represent any two points in the domain of the nonlinear function. Based on the general slip model defined in Eq. (5), we get

$$\mathbf{f}(\mathbf{z}) = \mathbf{B}_n f_s(\mathbf{z}) \tag{18}$$

The implication is that $\mathbf{f}(\mathbf{z})$ is Lipschitz if the scalar nonlinear function, f_s, describing slip dynamics is Lipschitz. Assuming that f_s is analytic (which is generally true for slip dynamics [1,24]), the Lipschitz constant, based on the consistency of the matrix one norm, can be derived as

$$\gamma \le \left\|\mathbf{B}_n\right\|_1 \max_{\mathbf{z}\in\Omega} \left\| \frac{\partial f_s}{\partial \mathbf{z}}(\mathbf{z}) \right\|_1 \tag{19}$$

where Ω is defined to be the set containing all states within the working range of the friction drive (which is bounded).

Table 3: Bounds on TFRD's States

Parameter	Value	Bounded States
Max. Travel Range [mm]	500	x_1, x_2
Max. Speed [mm/s]	100	$\dot{x}_1$, $\dot{x}_2$
Max. Feed Force [N]	200	F_t

To calculate the Lipschitz constant for the TRFD modeled in Section 2.3, the partial derivative of f_s is expressed as

$$\frac{\partial f_s}{\partial \mathbf{z}} = \frac{p}{l - pc\dot{x}_1}\begin{bmatrix} k\dot{x}_1 & -k\dot{x}_1 & F_t + c\dot{x}_1 & -c\dot{x}_1 & k\dot{x}_1 \end{bmatrix} \tag{20}$$

Note that all the terms in Eq. (20) except the third are calculated from Eq. (14); the third term is calculated from Eq. (11) as

$$\begin{aligned} \frac{\partial f_s}{\partial \dot{x}_1} &= \frac{p}{l}\left[F_t + c\dot{x}_1 \left(1 + \frac{\partial f_s}{\partial \dot{x}_1} \right) \right] \\ \Rightarrow \frac{\partial f_s}{\partial \dot{x}_1} &= \frac{p\left(F_t + c\dot{x}_1\right)}{l - pc\dot{x}_1} \end{aligned} \tag{21}$$

The bounds on the states of the TRFD of Fig. 2 are summarized in Tab. 3. Note that some of the bounds provided are conservative compared to those reported in [18] partly because, in this paper, only one actuator (i.e., the rotary motor) of the HFD is considered. Based on the values reported in Tabs. 1, 2 and 3, the Lipschitz constant for the TRFD modeled in Section 2.3 is bounded by

$$\gamma \le \left(\frac{c}{m_1} + \frac{c}{m_2} + 1 \right) \frac{p_2 k \left(\dot{x}_1\right)_{\max}}{l - p_2 c \left(\dot{x}_1\right)_{\max}} \tag{22}$$

In addition to the Lipschitz condition, it is important to ensure that the system dynamics cannot become singular due to the condition described by Eq. (15). Using the values of p, c and $\dot{x}_1$ given in Tabs. 1, 2 and 3, and noting that l = 5 mm, the relationship 4.25mm $\le l_0 \le$ 5.75mm is obtained, which guarantees the absence of singularities.

3.2 Observer Design and Slip Compensation

The extended Luenberger observer [22] is given by the equation

$$\begin{aligned} \dot{\hat{\mathbf{z}}} &= \mathbf{A}\hat{\mathbf{z}} + \mathbf{B}_u u + \mathbf{B}_n f_s(\hat{\mathbf{z}}) + \mathbf{L}\left(\mathbf{y} - \mathbf{C}_y \hat{\mathbf{z}}\right) \\ \mathbf{y}_s &\triangleq \begin{bmatrix} \hat{x}_s & 0 & \dot{\hat{x}}_s & 0 \end{bmatrix}^T \end{aligned} \tag{23}$$

where $\mathbf{L}$ is the linear observer matrix and $\mathbf{y}_s$ is the observer output; the ^ accent is used to denote an observed state. Notice that the extended Luenberger observer augments the traditional Luenberger observer with additional nonlinear terms. The observer design entails the selection of a matrix $\mathbf{L}$ that ensures

convergence. A convergence condition for **L** is proposed and proven in [22] based on the Lipschitz constant. The recursive algorithm proposed in [23] is used to automatically calculate **L**.

Using the slip observer output, $\mathbf{y}_s$, slip compensation is achieved by modifying the reference command, $\mathbf{y}_r$, as

$$\mathbf{y}_r = \begin{bmatrix} x_r & \dot{x}_r & \ddot{x}_r & \dddot{x}_r \end{bmatrix}^T - \mathbf{y}_s \tag{24}$$

where $\mathbf{y}_r = [y_{r1}, y_{r2}, y_{r3}, y_{r4}]^T$ is the compensated reference for states $[x_1, x_2, \dot{x}_1, \dot{x}_2]^T$, respectively. Depicting the operation of Eq. (24) by a slip compensation block, **Y**, the block diagram of the controller, including the slip observer and compensation, is shown in Fig. 7. The blocks enclosed by the blue dashed lines represent the plant (i.e., the two-mass model including slip dynamics). The control input, u, and plant outputs, **y**, are fed into the slip observer, generating estimated slip, $\mathbf{y}_s$, as defined in Eq. (23). Then $\mathbf{y}_s$ is used to compensate the reference, such that a linear controller **C**(s) can be used to control x_2 to track x_r effectively.

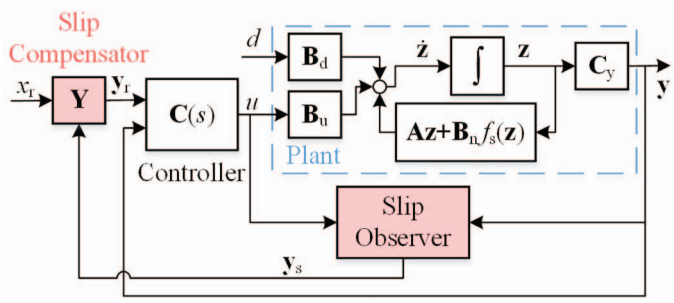

Figure 7: Block Diagram of Controller with Proposed Slip Observer and Compensation

4. SIMULATION AND EXPERIMENTS

In this section, the effect of the proposed slip compensation scheme is tested in simulations and experiments. The friction drive is required to track a snap-limited reference trajectory, x_r, illustrated in Fig. 8, where X_{lim} is the travel range, while V_{lim}, A_{lim}, J_{lim} and S_{lim} are the maximum velocity, acceleration, jerk and snap, respectively.

The general linear controller **C**(s) is assumed to be a state feedback controller given by

$$u = \mathbf{K}\begin{bmatrix} \int (y_{r2} - y_2)\,dt \\ y_{r1} - y_1 \\ y_{r2} - y_2 \\ y_{r3} - y_3 \\ y_{r4} - y_4 \end{bmatrix} \tag{25}$$

where **K** is a static feedback matrix. Note that an integrator state is added to ensure zero steady state positioning error even under load.

As mentioned in Section 2.1, the major problem introduced by slip is the accumulative position difference between x_1 and x_2. An intuitive means of compensating for the position difference is to employ a high pass filter (HPF) to eliminate the steady state portion of the accumulating error of x_1 before using it for feedback control. Here, x_1 is chosen for high pass filtering since x_2 is the state to be precisely tracked. This intuitive approach is included for the purposes of comparison with the proposed observer-based approach. In other words, three cases are compared:

i) Without compensation
ii) Using the proposed slip compensation scheme
iii) Using a HPF to eliminate the steady state portion of the accumulating error in x_1.

The three cases are compared with and without loads. In all simulations and experiments, the uniform linear model (i.e., using p_0) is employed. This is because, as shown in Tab. 1, the uniform linear model is not too far from the piecewise linear model with regard to accuracy. However, the use of the piecewise linear model introduces switching in the system dynamics which could cause undesirable transients and instability.

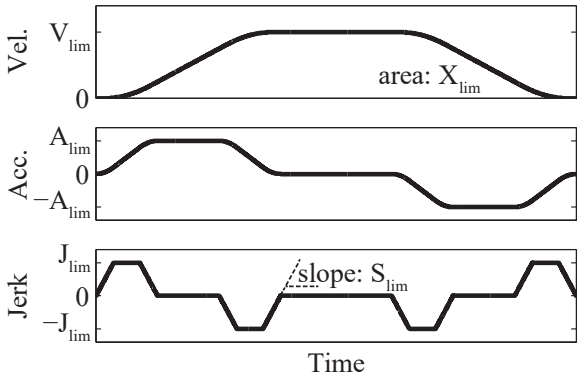

Figure 8: Snap Limited Trajectory

4.1 Simulations

The reference trajectory used in for simulations is defined by the trajectory parameters in Tab. 4. The state feedback controller **K** is calculated using the LQR technique, based on the linear two-mass model (i.e., without slip). The resulting **Q** and R weights are diag($[10^9,10^2,10^7,10^2,10^2]$) and 10^{-9}, respectively.

Table 4: Trajectory Parameters

X_{lim} [m]	V_{lim} [m·s^{-1}]	A_{lim} [m·s^{-2}]	J_{lim} [m·s^{-3}]	S_{lim} [m·s^{-4}]
0.01	0.01	0.1	6.25	1.25×10^{-5}

Figure 9 illustrates the tracking performance for the three cases under different loads. When there are only inertial loads, the steady state error in the constant velocity region for the schemes are almost the same; however, the proposed slip compensated case is better in terms of providing faster settling to constant velocity. When the external load is introduced, the differences in tracking performances become very clear, in that the no compensation case generates a constant steady state error. The slip term can be interpreted as a physical integrator; the accumulating error of state x_1 achieves a balance with the

integrator state of the controller, thus generating the steady state error. Unlike the no compensation case, the case with the proposed slip compensation almost has no performance degradation with load. The HPF approach is shown to be capable of slowly dealing with slip. However, the cutoff frequency of the HPF is very sensitive to the input trajectory and closed loop system dynamics; increasing the cut off frequency of the HPF can easily destabilize the system.

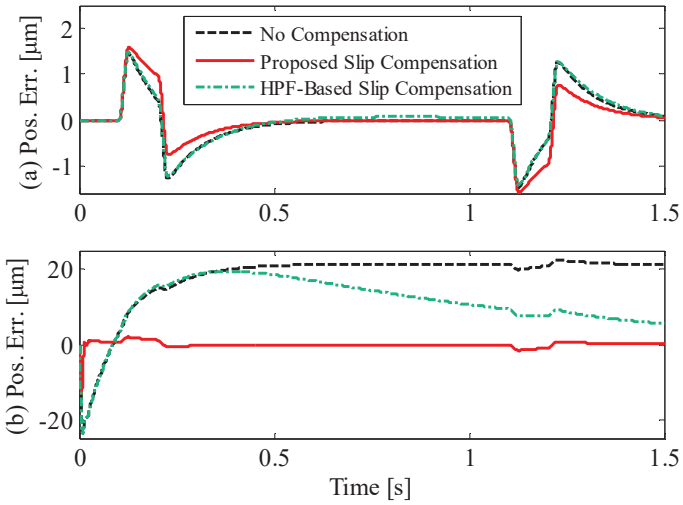

Figure 9: Comparison of Positioning Performance of Proposed Slip Compensation with the No Compensation and HPF-Based Compensation Cases for (a) No Disturbance, (b) with Disturbance *d* = 100N (Simulation)

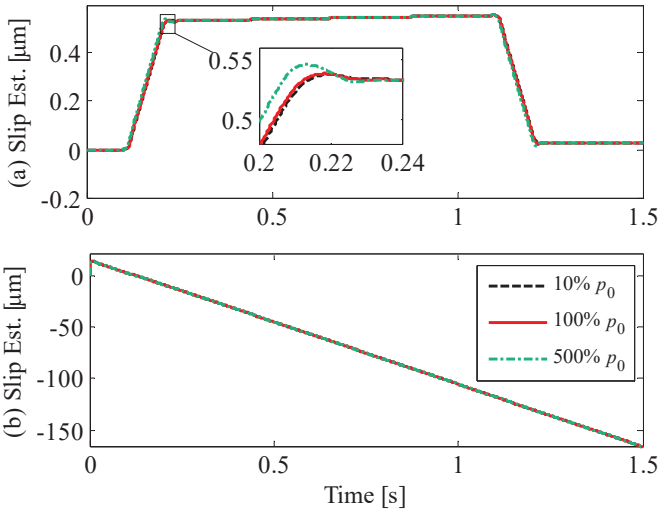

Figure 10: Robustness of Slip Estimation in the Presence of Slip Coefficient Variation with (a) No Disturbance (b) with Disturbance *d* = 100N

Figure 10 illustrates the robustness of the slip estimation in the presence of variations in slip coefficient, with and without load. The slip estimation is shown to be robust, in that even five times the nominal value only causes 2 % overshoot in slip estimation. This also justifies the use of the linear slip model as opposed to the piecewise linear model.

4.2 Experiments

In this section, the effect of the proposed method is validated through experiments. The same trajectory as in the simulation, whose parameters provided in Tab. 4, is used. The controller is tuned using the P-PI control loop as proposed in [18]. Note that the P-PI controller is equivalent to a state feedback controller (according to Eq. (25)), in this particular case, with $\mathbf{K} = [9.1\times10^7, 4.6\times10^7, 5.2\times10^5, 2.6\times10^5, 0]$.

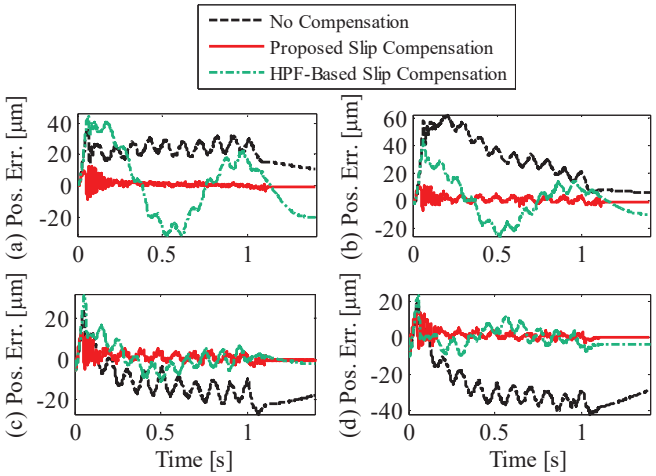

Figure 11: Comparison of Positioning Performance of Proposed Slip Compensation with the No Compensation and HPF-Based Compensation Cases for (a) No External Load, and with External Load of (b) F_L = 20N, (c) F_L = 40N, (d) F_L = 60N (Experiment)

In Fig. 11, the positioning performances in the three cases are compared in experiments using various loading scenarios. The linear motor is used to adjust disturbance by incremental change of F_L. It is shown that the proposed slip compensation method has the best tracking accuracy in all cases, and its tracking errors are least influenced by the external loads. The case with no slip compensation, on the contrary, accumulates errors due to slip as the external load increases. The positioning accuracy of the HPF approach is enhanced as the load increases. This is because the low frequency portion of x_1, which is discarded by the HPF, is better damped with increased loads (tension) on the transmission. Nonetheless, its tracking performance is still inferior to that of the proposed slip compensation method.

5. CONCLUSION AND FUTURE WORK

This paper addresses the problem of deterioration of positioning accuracy due to slip in servo positioners equipped with continuous friction drives. A general two-mass model that

includes slip dynamics is presented and experimentally identified for a precision servo positioner equipped with a twist-roller friction drive. Using the model, a nonlinear observer is designed to observe and compensate slip, based on feedback from driving and driven sides of the friction drive. Simulations and experiments are used to show that the proposed method significantly enhances servo positioning accuracy compared to a controller without slip compensation, and one with an intuitive high pass filter based slip compensator. The proposed method is also shown to be robust to load and slip coefficient variation. Future work will investigate observer-based slip compensation for the redundantly-actuated hybrid feed drive described in the paper (i.e., with its linear and rotary motor actuation combined).

ACKNOWLEDGMENT

This work is funded by the National Science Foundation's CAREER Award #1350202: Dynamically Adaptive Feed Drives for Smart and Sustainable Manufacturing.

REFERENCES

[1] Sanda, S., and Hayakawa, K., 2005, "Traction drive system and its characteristics as power transmission," R&D Rev. Toyota CRDL, **40**(3), pp. 30–39.

[2] Stammes, C. W., Prest, P. H., and Mobley, C. G., 1992, "A friction drive robot wrist: electronic and control requirements," Mechatronics, **2**(4), pp. 391–401.

[3] Mizumoto, H., Nomura, K., Matsubara, T., and Shimizu, T., 1993, "An ultraprecision positioning system using a twist-roller friction drive," Precis. Eng., **15**(3), pp. 180–184.

[4] Srinivasan, K., and Tsao, T. C., 1997, "Machine Tool Feed Drives and Their Control—A Survey of the State of the Art," J. Manuf. Sci. Eng., **119**(4B), p. 743.

[5] Chang, W. S., and Youcef-Toumi, K., 1998, "Modeling of an omni-directional high precision friction drive positioning stage," Proceedings. 1998 IEEE International Conference on Robotics and Automation, IEEE, pp. 175–180.

[6] Wang, G., Ma, L., Yao, Z., and Li, G., 2004, "Experiment study on friction drive," Astronomical Telescopes and Instrumentation, J. Antebi, and D. Lemke, eds., International Society for Optics and Photonics, pp. 419–428.

[7] Gao, W., Sato, S., and Arai, Y., 2010, "A linear-rotary stage for precision positioning," Precis. Eng., **34**(2), pp. 301–306.

[8] Panusittikorn, W., Lee, M. C., and Ro, P. I., 2004, "Modeling and sliding-mode control of friction-based object transport using two-mode ultrasonic excitation," IEEE Trans. Ind. Electron., **51**(4), pp. 917–926.

[9] Kim, S.-C., and Kim, S. H., 2001, "A precision linear actuator using piezoelectrically driven friction force," Mechatronics, **11**(8), pp. 969–985.

[10] Mekid, S., 2009, "Precision design aspects for friction actuation with error compensation," J. Mech. Sci. Technol., **23**(11), pp. 2873–2884.

[11] Mizumoto, H., Yabuya, M., Shimizu, T., and Kami, Y., 1995, "An angstrom-positioning system using a twist-roller friction drive," Precis. Eng., **17**(1), pp. 57–62.

[12] Pulles, R. J., Bonsen, B., Steinbuch, M., and Veenhuizen, P. a., 2005, "Slip controller design and implementation in a continuously variable transmission," Proc. 2005, Am. Control Conf. 2005., pp. 1625–1630.

[13] Sinha, S. K., Thia, S. L., and Lim, L. C., 2007, "A new tribometer for friction drives," Wear, **262**(1-2), pp. 55–63.

[14] Yang, S., and Zhang, Z., 2008, "Servo control system for friction drive with ultra-low speed and high accuracy," Proc. SPIE, **7019**, p. 70192B–70192B–8.

[15] Lee, Y.-S., 2011, "Comparison of collocation strategies of sensor and actuator for vibration control," J. Mech. Sci. Technol., **25**(1), pp. 61–68.

[16] Lee, R.-T., Chiou, Y.-C., and Lin, Y.-W., 1999, "Study on slip displacement and stick-slip characteristics in reciprocating friction drive system," Tribol. Int., **32**(2), pp. 97–106.

[17] Frącczak, Ł., Podsędkowski, L. R., and Zawierucha, M., 2011, "The servo drive with friction wheels," J. Autom. Mob. Robot. Intell. Syst., **5**, pp. 14–20.

[18] Okwudire, C., and Rodgers, J., 2013, "Design and control of a novel hybrid feed drive for high performance and energy efficient machining," CIRP Ann. - Manuf. Technol., **62**(1), pp. 391–394.

[19] Boukhezzar, B., and Siguerdidjane, H., 2011, "Nonlinear Control of a Variable-Speed Wind Turbine Using a Two-Mass Model," IEEE Trans. Energy Convers., **26**(1), pp. 149–162.

[20] Duan, M., and Okwudire, C., 2015, "Energy-efficient Controller Design for a Redundantly-actuated Hybrid Feed Drive with Application to Machining," IEEE/ASME Trans. Mechatronics.

[21] Chen, J.-S., Chen, K.-C., Lai, Z.-C., and Huang, Y.-K., 2003, "Friction characterization and compensation of a linear-motor rolling-guide stage," Int. J. Mach. Tools Manuf., **43**(9), pp. 905–915.

[22] Thau, F. E., 1973, "Observing the state of non-linear dynamic systems," Int. J. Control, **17**(3), pp. 471–479.

[23] Raghavan, S., and Hedrick, J. K., 1994, "Observer design for a class of nonlinear systems," Int. J. Control, **59**(2), pp. 515–528.

[24] Yang, C.-R., Chiou, Y.-C., and Lee, R.-T., 1995, "Study on positioning accuracy of reciprocating friction drive system," Wear, **189**(1-2), pp. 58–65.